The Astrophysical Journal, 575:814–825, 2002 August 20

MOLECULAR GAS IN CANDIDATE DOUBLE-BARRED GALAXIES. I. THE DIVERSE MORPHOLOGY AND DYNAMICS OF NGC 2273 AND NGC 5728

Glen R. Petitpas[1] and Christine D. Wilson
Department of Physics and Astronomy, McMaster University, 1280 Main Street West, Hamilton, ON L8S 4M1, Canada;
petitpas@physics.mcmaster.ca, wilson@physics.mcmaster.ca
Received 2001 June 8; accepted 2002 April 19

ABSTRACT

Double bars have been proposed as a means of transporting molecular gas past inner Lindblad resonances into the nuclear regions, where it can fuel active or starburst nuclei. Thus far, the existence of double bars has been determined predominantly through analysis of near-infrared images, which can tell us little about the dynamics and inflow rates of these systems. We have observed two double-bar galaxy candidates (NGC 2273 and NGC 5728) in ^{12}CO $J = 1$–0 with the Owens Valley Radio Observatory Millimeter Array. Despite the similarity in the near-infrared images of these galaxies, we see rather different nuclear morphologies in the CO maps. NGC 2273 shows evidence of a nuclear gas bar, aligned with the nuclear stellar bar seen in the near-infrared images. Both the nuclear gaseous and the stellar bars are misaligned from the large-scale bar by $\sim 90^\circ$, which also allows the possibility that both are the result of stars and gas populating the x_2 orbits of the primary bar. Estimates using dynamical friction arguments and star formation rates suggest significant gas inflow rates along the nuclear bar of NGC 2273. Conversely, NGC 5728 does not show any evidence for a nuclear molecular bar but shows an arc of CO clumps that peaks just to the southwest of the dynamical center and curves to the southeast, where it follows the dust lane to the south. Models of double-barred galaxies suggest that these galaxies should contain large amounts of molecular gas in their nuclei. Our calculations suggest that both galaxies contain sufficient amounts of gas in their nuclei, but only NGC 2273 shows evidence for a nuclear gas bar. This may be the result of past episodes of star formation exhausting and dispersing the nuclear gas of NGC 5728, but it is more likely evidence that NGC 5728 has undergone a minor merger event.

Subject headings: galaxies: active — galaxies: individual (NGC 2273, NGC 5728) — galaxies: ISM — galaxies: kinematics and dynamics — galaxies: nuclei — galaxies: starburst

1. INTRODUCTION

The nuclei of barred spiral galaxies are often the setting for extraordinary events, such as starbursts, molecular rings, inflow, and even Seyfert activity. The need to understand the mechanisms driving these phenomena has inspired a great number of observations and computer simulations. Models suggest that bars in galaxies can drive molecular gas into the nuclear regions, where it can fuel the vigorous star formation activity that would otherwise exhaust the molecular gas content on timescales much shorter than observed (e.g., Combes 1994). Bars can only drive molecular gas inward until it approaches the inner Lindblad resonance (ILR; see Fig. 1), where it will halt its inflow and accumulate into a ring. To overcome this, Shlosman, Frank, & Begelman (1989) proposed that the ring may become unstable and form a secondary bar inside the radius of the ILR, which could allow gas to reach much farther into the nucleus and possibly be the driving mechanism behind Seyfert nuclei.

Recent near-infrared (NIR) surveys reveal isophote twists in the central regions of barred galaxies, which may be the signature of this "bar within a bar" (e.g., Mulchaey, Regan, & Kundu 1997). There are three mechanisms that can account for NIR isophotal twists (Elmegreen et al. 1996). The first mechanism (hereafter called model 1), proposed by Shaw et al. (1993), suggests that the isophote twists are the result of twisting of the primary bar triggered by a dissipative gaseous component and misaligned from the primary bar. Their numerical simulations suggest that in the presence of two ILRs, a nuclear ring can become elongated perpendicular to the primary bar (along the x_2 orbits). Gas dissipation causes the inner part of the perpendicular gaseous ring to become more aligned with the primary bar, resulting in the appearance of an elongated nuclear ring that leads the primary bar. This gas ring exerts a torque on the stellar component of the bar, pulling it out of alignment also. The whole system would then rotate with the same angular frequency, with the inner gaseous ring and inner part of the primary bar leading the outer parts of the primary bar. The second mechanism (hereafter model 2) suggests that the twists are the result of a kinematically distinct secondary bar (Friedli & Martinet 1993). Their N-body simulations (with stars and gas) suggest that gas inflow along the primary bar can accumulate enough mass that the inner part of the gas bar can become nearly self-gravitating and decouple from the primary bar. The secondary bar may rotate with a pattern speed of up to 6 times that of the primary bar. The third mechanism (model 3) suggests that the NIR isophote twists may be the result of a triaxial stellar bulge (Kormendy 1979).

Detailed analyses of NIR images reveal that in many cases, these isophote twists must be caused by the existence of true nuclear stellar bars (Friedli et al. 1996; Jungwiert, Combes, & Axon 1997). Typically, nuclear stellar bars are identified by two distinct peaks in the plots of ellipticity versus radius, as well as a sudden change in the position angle of the isophotes at the end of the nuclear bar (unless the nuclear and large-scale bars are aligned; Wozniak et al.

[1] Current address: Department of Astronomy, University of Maryland, College Park, MD 20742.

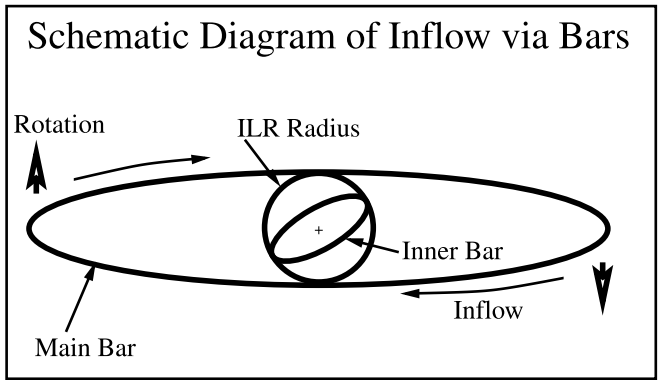

FIG. 1.—Schematic diagram of how a large-scale bar (main bar) passing through a disk can transport material toward the nucleus of the galaxy. It is difficult for simulations to transport material all the way to the center because it tends to get trapped at the inner Lindblad resonance (ILR). This figure shows the inner bar that may form interior to the ILR and transport material all the way to the nucleus.

1995). Unfortunately, even at NIR wavelengths, dust obscuration and contamination by young red supergiants in regions of star formation in the nuclei of these galaxies with isophote twists can make it difficult to identify nuclear bars unambiguously (e.g., Friedli et al. 1996; Rhoads 1998). Fortunately, since molecular gas observations in the millimeter and submillimeter regime are not prone to dust extinction, observations of ^{12}CO $J = 1$–0 can be used to probe the morphology and dynamics of the molecular gas in these nuclei.

The three competing explanations for the NIR isophote twists can also be tested using these molecular gas observations. Model 1 would exhibit a secondary gaseous bar that may lead the secondary stellar bar slightly but has the same rotation speed as the primary bar. Model 2 would show a gaseous secondary bar that is rotating with a different pattern speed than the primary bar. Thus, molecular gas dynamics should allow us to distinguish between these models. Model 3 is associated with the stellar bulge. Since there is very little gas in the bulge compared to the disk of a galaxy, the CO maps need not resemble the NIR images. If the CO maps do share similar features with the NIR images, it may suggest that the isophote twists are related to the disk of the galaxy and not the bulge. Both the first and the second models were only able to re-create relatively long-lived (i.e., a few $\times 10^8$ yr) nuclear NIR isophote twists in models that contained sufficient amounts of molecular gas (initially 2%–10% gas globally, higher in the nuclear regions at later stages of evolution). Without these high gas fractions, there is not enough dissipation in the models, and the observed structures do not last long enough to be as common as they are observed to be (Shaw et al. 1993; Friedli & Martinet 1993).

Previous CO studies of galaxies with nuclear stellar bars have revealed a variety of CO morphologies, but most show some evidence for a nuclear gas bar. Perhaps the current best example of a galaxy with nuclear gaseous and stellar bars is NGC 2782 (Jogee, Kenney, & Smith 1999). The NIR images of this galaxy show evidence for a nuclear stellar bar in the ellipticity of the isophotes. The CO map for this galaxy resembles a twin peaked morphology, with the twin peaks of CO emission aligned with the nuclear stellar bar. The CO data show kinematic evidence for inflow along the nuclear bar. Estimates of the inflow rates for NGC 2782 suggest values that are high enough to sustain the star formation rates of $\sim$3–6 $M_\odot$ yr^{-1} for approximately 5×10^8 yr.

Previous studies of M100 have shown the existence of both a nuclear stellar bar and a nuclear gas bar. Garcia-Burillo et al. (1998) modeled the large- and small-scale H I and CO observations using a variety of numerical models and found that the best fit to the observations was for the case of a kinematically distinct nuclear bar rotating at nearly 7 times the pattern speed of the large-scale bar. The kinematically distinct nuclear bar was needed in the models to create enough inflow to reproduce the high concentration of gas seen in the nuclear disk of M100. Unfortunately, no estimates of the inflow rate are given.

Studies of NGC 4736 by Wong & Blitz (2000) show a nuclear gas bar roughly aligned with the nuclear stellar bar seen in the NIR images by Shaw et al. (1993). The CO maps show evidence for inflow rates of $\sim$2 $M_\odot$ yr^{-1} for the outer bar, but no estimates for inflow rates along the nuclear bar are given. Presumably, these rates would have to be on the order of at least 0.2 $M_\odot$ yr^{-1} to sustain the nuclear star formation rates.

In other cases, there is evidence for a nuclear gas bar when there is no evidence for a nuclear stellar bar. For example, NGC 3351 (Devereux, Kenney, & Young 1992) was the first galaxy to show a molecular gas bar perpendicular to the large-scale stellar bar. Unfortunately, Devereux et al. (1992) did not resolve the bar across its minor axis, so they are unable to determine if there are kinematic signatures of inflow. Later studies of this galaxy suggest that the nuclear gas bar is simply the gas collecting at ILRs (Kenney et al. 1992).

This paper presents observations taken with the Owens Valley Radio Observatory Millimeter Array of two galaxies that exhibit NIR isophote twists: NGC 2273 and NGC 5728. NGC 2273 is a SB(r)a galaxy that has a Seyfert 2 nucleus, nuclear star formation (Mulchaey, Wilson, & Tsvetanov 1996), and a nuclear ring of dust ($r \approx 5''$; Yankulova 1999). It has a recession velocity of 1841 km s^{-1} (de Vaucouleurs et al. 1991), which implies that it is 24.5 Mpc away (assuming $H_0 = 75$ km s^{-1} Mpc^{-1}). It also has three outer rings that appear to be made by separate sets of spiral arms at $r \approx 0.'4$, $1.'1$, and $1.'0$. H I observations indicate that it is not very gas rich for a barred spiral galaxy with such a wide variety of nuclear activity (van Driel & Buta 1991). This observation is supported by the ^{12}CO $J = 1$–0 spectra taken by Young & Devereux (1991), who find very narrow CO line widths and conclude that most of the molecular gas must be contained in the central few arcseconds of the nuclei of NGC 2273. Color maps of the inner regions of NGC 2273 suggest that there is a reddened ring of dusty material ($r \sim 5''$) surrounding a region of high ionization (Yankulova 1999). NGC 5728 is a southern hemisphere barred spiral galaxy classified as SAB(r)a that also contains a Seyfert 2 nucleus. Its recession velocity of 2788 km s^{-1} (de Vaucouleurs et al. 1991) suggests that it is located at a distance of 37.2 Mpc. Color maps indicate that the galaxy contains two blue rings of recent star formation, one in the nucleus ($r \approx 5''$; Wilson et al. 1993) and one near the primary bar ends ($r \approx 55''$; Schommer et al. 1988). Two dust lanes emerge from just outside the nuclear ring and run parallel to the primary bar of the galaxy. Table 1 summarizes the properties and adopted parameters for these galaxies. These two

TABLE 1
ADOPTED PROPERTIES OF NGC 2273 AND NGC 5728

Property	NGC 2273	NGC 5728	References
R.A. (2000.0)	$06^h50^m08^s.7$	$14^h42^m24^s.0$	1
Decl. (2000.0)	$+60°50'45''.1$	$-17°15'10''.8$	1
Classification	SB(r)a	SAB(r)a	2
Optical diameter	$3'.3$	$3'.1$	1, 2
Nuclear ring diameter	$\sim 10''$	$\sim 10''$	3, 4
Outer ring diameter(s)	$0'.7$, $2'.2$, $3'.1$	$55''$	4, 5
Inclination	41°	48°	2, 4
Primary bar P.A.	$\sim 115°$	$\sim 38°$	4, 6
NIR isophote twist P.A.	$\sim 45°$	$\sim 90°$	6, 7
Heliocentric velocity	1841 km s^{-1}	2788 km s^{-1}	2
Assumed distance	24.5 Mpc	37.2 Mpc	8
Linear scale	$1'' = 120$ pc	$1'' = 180$ pc	8

REFERENCES.—(1) NASA/IPAC Extragalactic Database; (2) de Vaucouleurs et al. 1991; (3) Yankulova 1999; (4) Schommer et al. 1988; (5) van Driel & Buta 1991; (6) Mulchaey et al. 1997; (7) Shaw et al. 1993; (8) assumes $H_0 = 75$ km s^{-1} Mpc^{-1}.

galaxies were chosen as targets for this study because of the similarity in their nuclear and large-scale morphologies; both galaxies are classified as Seyfert 2 galaxies and contain nuclear rings (which suggest the presence of at least one ILR), and, most importantly, both galaxies exhibit the NIR isophote twists that may be the signature of a nuclear bar, as discussed above.

In § 2 we discuss the observations and data reduction techniques. In § 3 we discuss the molecular gas distribution and dynamics. In § 4 we discuss the molecular gas mass determined from the ^{12}CO $J = 1$–0 flux in comparison with the amount of molecular gas required by the models to produce the observed features. In § 5 we search for signs of inflow in NGC 2273 and compare these with star formation rates. In § 6 we compare our results with models of double-barred galaxies and previous observations of these galaxies. In § 7 we discuss our observations in relation to observations of other galaxies thought to contain nuclear stellar and gaseous bars. The paper is summarized in § 8.

2. OBSERVATIONS AND DATA REDUCTION

We have observed the barred galaxies NGC 2273 and NGC 5728 in ^{12}CO $J = 1$–0 (115.3 GHz) using the Owens Valley Radio Observatory Millimeter Array. For NGC 2273, we have three tracks, two in the low-resolution (L) configuration and one in the high-resolution (H) configuration. For NGC 5728, we have four tracks (two in H, one in L, and one in the equatorial [E] configuration). Preliminary calibration was done using the calibration package MMA (Scoville et al. 1993). Only data with a coherence greater than 0.5 were used. The quasars 0642+449 and 1334−127 were used for gain calibration, and Neptune and 3C273 were used for flux calibration.

For NGC 2273, we used $\alpha(2000) = 06^h50^m08^s.7$, $\delta(1950) = +60°50'45''.1$ for the pointing center (note that this is slightly different from the galactic center), and the spectrometer was centered at $V_{lsr} = 1841$ km s^{-1}. For NGC 5728, we used the pointing center of $\alpha(2000) = 14^h42^m24^s.0$, $\delta(2000) = -17°15'10''.8$ and a recession velocity of $V_{lsr} = 2930$ km s^{-1}. In both cases, the spectrometer had a bandwidth of 240 MHz, which corresponds to a velocity coverage of $\sim$620 km s^{-1}. The frequency resolution was 2 MHz, which gives a velocity resolution of 5.2 km s^{-1} at 115 GHz; however, we have binned the data to a resolution of 10.4 km s^{-1} to increase the signal-to-noise ratio.

For mapmaking, we used the data reduction software MIRIAD (Sault, Teuben, & Wright 1995). Data with unusually high visibilities were clipped, the maps were naturally weighted, and the inner quarter CLEANed to 1 σ. The resulting synthesized beam is $3''.0 \times 2''.5$ (P.A. = 21°) for NGC 2273 and $4''.5 \times 3''.0$ (P.A. = −12°) for NGC 5728. The rms noise in the maps is 3.09 Jy beam^{-1} km s^{-1} for NGC 2273 and 2.65 Jy beam^{-1} km s^{-1} for NGC 5728. The maps cover a $60'' \times 60''$ area, but only the regions with significant emission are shown in Figures 2 and 5.

3. MOLECULAR GAS DISTRIBUTION, DYNAMICS, AND COMPARISONS TO MODELS

3.1. *Morphology*

Figure 2 shows the NIR image (*top panel*) of Mulchaey et al. (1997), as well as the integrated intensity ^{12}CO $J = 1$–0 map (*bottom panel*) for NGC 2273. The CO emission is integrated over the velocity range in which we see emission, namely from 1669 to 1981 km s^{-1}. The ^{12}CO $J = 1$–0 integrated intensity map (Fig. 2) shows a small barlike structure (P.A. $\sim$ 40°) that is approximately perpendicular to the primary bar of the galaxy (P.A. $\sim$ 115°). Comparing the size of the CO bar with the synthesized beam, we see that the bar is resolved along its major axis but may not be fully resolved along its minor axis. The integrated intensity map also shows finger-like structures protruding to the north and south of the CO bar. Assuming trailing spiral arms, these fingers line up with the leading edge of the primary galactic bar.

The integrated intensity map shows only a two-dimensional view. If we want to see the details of how the molecular gas is distributed, we must use the velocity information. The channel maps (Fig. 3) show that the CO bar is actually three dynamically separate clumps that merge into a barlike structure when we average the emission over all channels. In order to emphasize the three individual clumps, we have used the CLUMPFIND algorithm (Williams, de Geus, & Blitz 1994) and plotted the individual clumps in Figure 4.

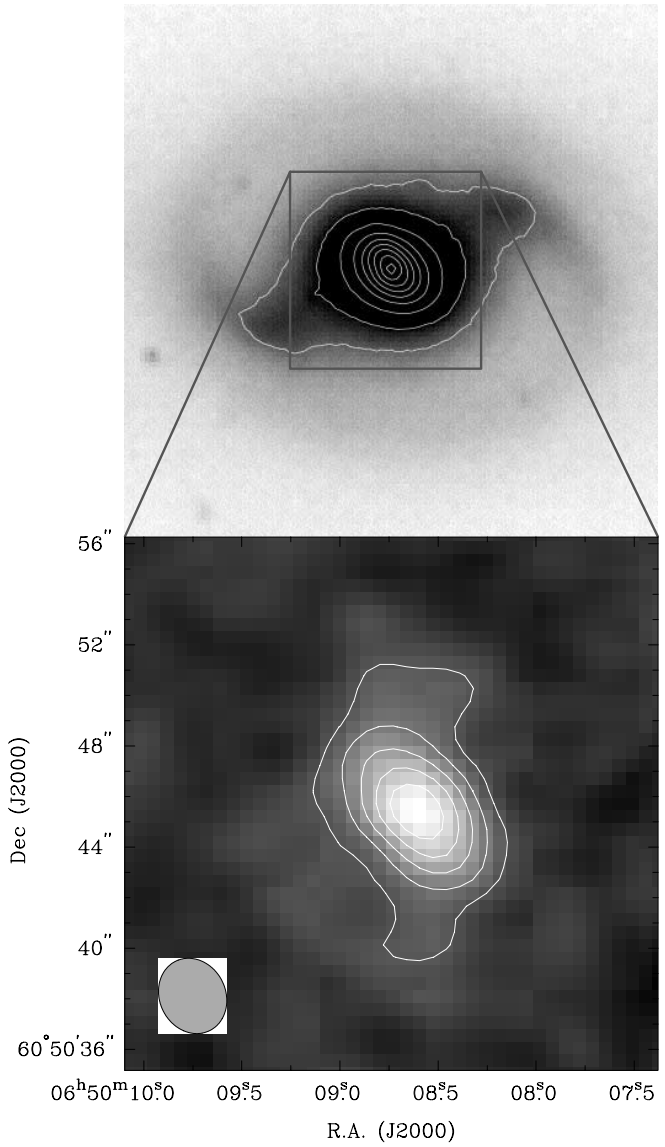

FIG. 2.—Integrated intensity map of ^{12}CO $J = 1$–0 emission in NGC 2273. The CO map of NGC 2273 (*bottom panel*) shows a nuclear bar aligned with the NIR isophote twists of Mulchaey et al. (1997; *top panel*). The fingers of emission to the north and south of the nuclear CO bar suggest evidence of inflow onto the secondary bar along the leading edge of the primary bar. In the NIR image, the contours start at 17 mag arcsec^{-2} (K_S band) and are in 0.5 mag increments. The rms noise in the CO map is 3.1 Jy beam^{-1} km s^{-1}, and the contour levels for the CO integrated intensity map start at 1 σ and increase in steps of 1 σ. The beam size of $3'' \times 2''.5$ with a P.A. of 21° is shown in the lower left corner.

The two clumps near the ends of the CO bar are brighter than the central peak, which suggests that molecular gas may be flowing in along the primary bar but is actually being collected into clumps that are presumably the location of the ILR. Similar CO morphologies have been seen in other barred galaxies, such as the "twin peaks" galaxies of Kenney et al. (1992) and the nearby starburst galaxy M82 (e.g., Shen & Lo 1995). We discuss the importance of these similarities in § 7.

The NIR image of NGC 2273 (Fig. 2, *top panel*; Mulchaey et al. 1997) shows isophote twists in the inner $10'' \times 10''$ misaligned from the primary bar by ~90°. The ^{12}CO $J = 1$–0 integrated intensity map (Fig. 2; *bottom panel*) shows a nuclear barlike structure that aligns with the position angle of the twisted NIR isophotes. Since we observe a similar morphology in the CO map and in the NIR image, it strongly suggests that the NIR isophote twists are the result of a disk phenomenon (as predicted by models 1 and 2) rather than a bulge phenomenon (model 3). The models of Shaw et al. (1993) predict that we should see the nuclear molecular component leading the nuclear isophote twists observed in the NIR by up to 20°. The models of Friedli & Martinet (1993) predict that the gaseous nuclear bar leads the gaseous stellar bar by up to ~20°. In NGC 2273, there is no clear evidence that the gaseous secondary bar is leading the stellar secondary bar by any significant amount. However, this observation does not rule out either model, since Shaw et al. (1993) and Friedli & Martinet (1993) predict deviation angles between the gaseous and stellar bars as small as 5°, which is smaller than we can measure accurately from the maps.

Figure 5 shows the *I*-band image (*top panel*) of Prada & Gutiérrez (1999), as well as the integrated intensity ^{12}CO $J = 1$–0 map (*bottom panel*) of NGC 5728. The CO emission is integrated over the velocity range of 2650–2980 km s^{-1}. The ^{12}CO $J = 1$–0 map of NGC 5728 (Fig. 5) does *not* show an obvious nuclear bar as seen in NGC 2273. It contains several individual clumps of emission that seem to form an arc with a radius of 6″. If this arc is part of a molecular ring, then the CO ring is not aligned with the galactic center, nor is it aligned with the ring structure surrounding ionization cones seen in the *Hubble Space Telescope* (*HST*) images by Wilson et al. (1993). The brightest peak in the CO map of Figure 5 is located ~2″ to the southwest of the brightest peak seen in the Very Large Array (VLA) and Hα maps of Schommer et al. (1988). The smaller CO clumps that run counterclockwise to the southeast of the brightest peak line up with the dust lane that runs out of the nucleus and along the primary bar of the galaxy (Schommer et al. 1988). We reserve discussion of the physical interpretation of these features for § 6.2.

At first glance, it appears that our CO map is offset from the galaxy center (marked with a plus sign in Fig. 5) determined by Schommer et al. (1988). It should be noted that the spectral lines in the nucleus of NGC 5728 cover such a large range of velocities that we have missed velocities lower than 2630 km s^{-1}. The Hα maps of Schommer et al. (1988) show that there are some velocities as low as 2600 km s^{-1} and as high as 3010 km s^{-1} in the nucleus of NGC 5728. The lowest velocity regions are located to the northeast of the dynamical center, so that if there is strong CO emission at 2600–2630 km s^{-1}, we will have missed it in our maps, perhaps creating the observed nonsymmetric appearance. There is definitely evidence of bright CO emission near the low-velocity end of our spectrometer. It can be seen as a faint peak in Figure 5 at R.A. = $14^h42^m24^s.2$, $\delta = -17°15'07''.6$ (it is the northeast clump that is used in the dynamical mass calculation of § 3.2).

To test whether the asymmetry seen in the CO map of NGC 5728 is caused by the exclusion of the lowest 30 km s^{-1} of the spectral data, we cropped the highest 30 km s^{-1} from the spectra and recreated the moment maps. This process reduces the intensity of the brightest peak to the west of the dynamical center, but the peak is still more than twice as bright as the emission peak on the northeast side of the dynamical center. Thus, it is likely that the asymmetric

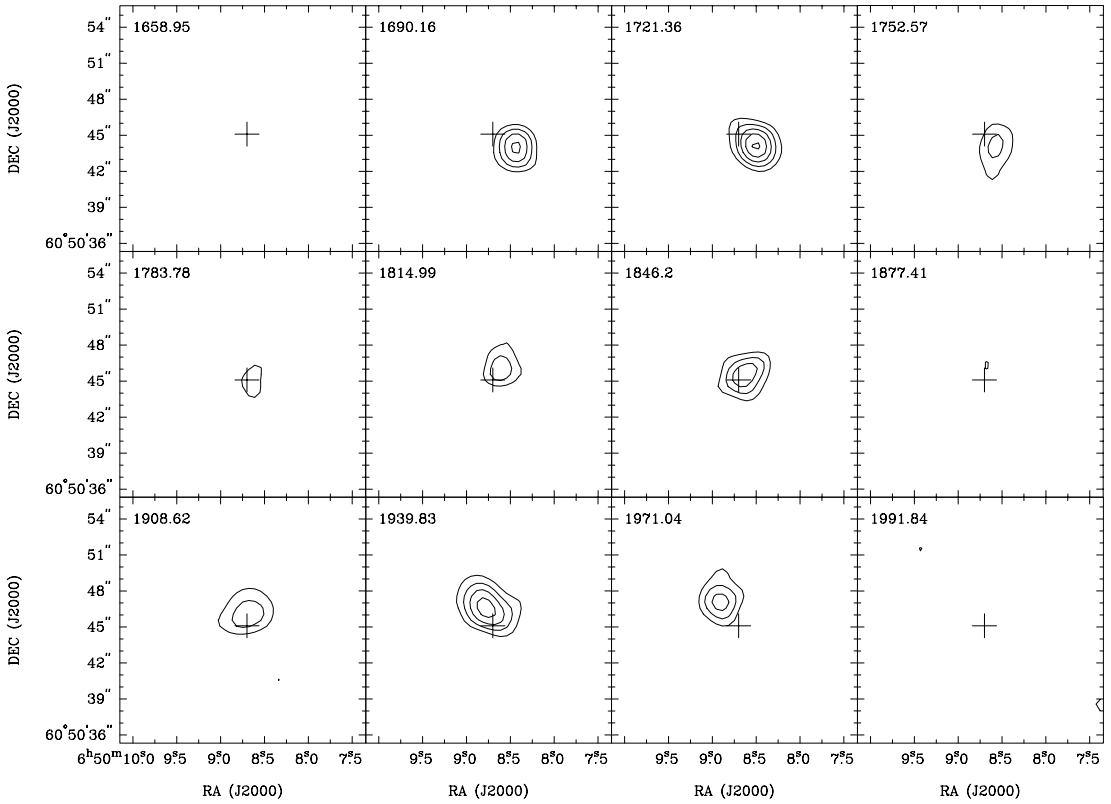

FIG. 3.—Channel maps of CO emission in NGC 2273. The CO bar seen in Fig. 2 is actually composed of three clumps. The contour levels are 0.04, 0.06, 0.08,... Jy beam^{-1} (2, 3, 4,... σ). The plus sign indicates the map center. The panels are shown at 31.2 km s^{-1} intervals and are binned to 31.2 km s^{-1} wide bins.

appearance of the CO map is real and not an artifact of missing low-velocity emission.

The NIR image of NGC 5728 (Fig. 5; see also Shaw et al. 1993) shows isophote twists in the nuclear region similar to those of NGC 2273, but our CO map of NGC 5728 shows no clear evidence for the existence of a nuclear bar. This result suggests that in NGC 5728, the NIR isophote twists may not be the result of the nuclear bar but may be caused by a triaxial stellar bulge as predicted by Kormendy (1979). The asymmetric CO distribution may also be evidence for a past merger event in NGC 5728. We give a more detailed discussion of the possible causes of the NIR isophote twists and discuss causes for the asymmetric gas distribution in § 6.2.

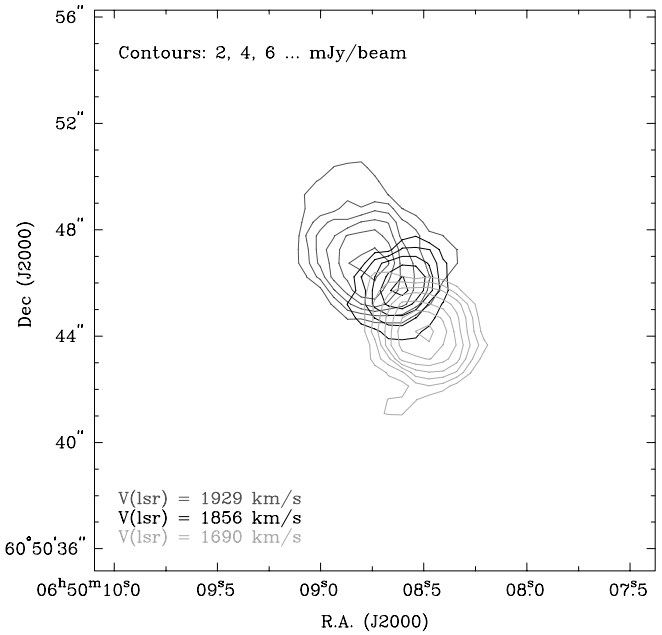

FIG. 4.—Clumps of CO emission that form the nuclear bar of NGC 2273. This figure shows the output from the CLUMPFIND algorithm. It shows the three main clumps of CO emission that combine to produce the bar seen in the integrated intensity map (Fig. 2).

3.2. *Dynamics*

The position-velocity diagram (Fig. 6) taken along the axis of the CO bar in NGC 2273 shown in Figure 2 indicates that the bar has a velocity gradient of ≈600 km s^{-1} kpc^{-1} (∼900 km s^{-1} kpc^{-1} deprojected). Since we have no detections beyond the secondary bar shown in Figure 2, and there are no rotation curves published for the inner 1′, we cannot determine yet if the CO secondary bar is kinematically distinct, as predicted by model 2, or if it is rotating at the same angular frequency as the primary bar, as predicted by model 1. In addition, without published rotation curves for the region just beyond the nuclear bar, we are unable to estimate the nuclear bar pattern speed.

Assuming Keplerian rotation, we have

$$M_{\rm dyn} = \left(\frac{V_{\rm circ}}{\sin i}\right)^2 \left(\frac{R}{G}\right),$$

where $M_{\rm dyn}$ is the mass interior to radius R, $V_{\rm circ}$ is the projected circular velocity of the material at radius R, i is the

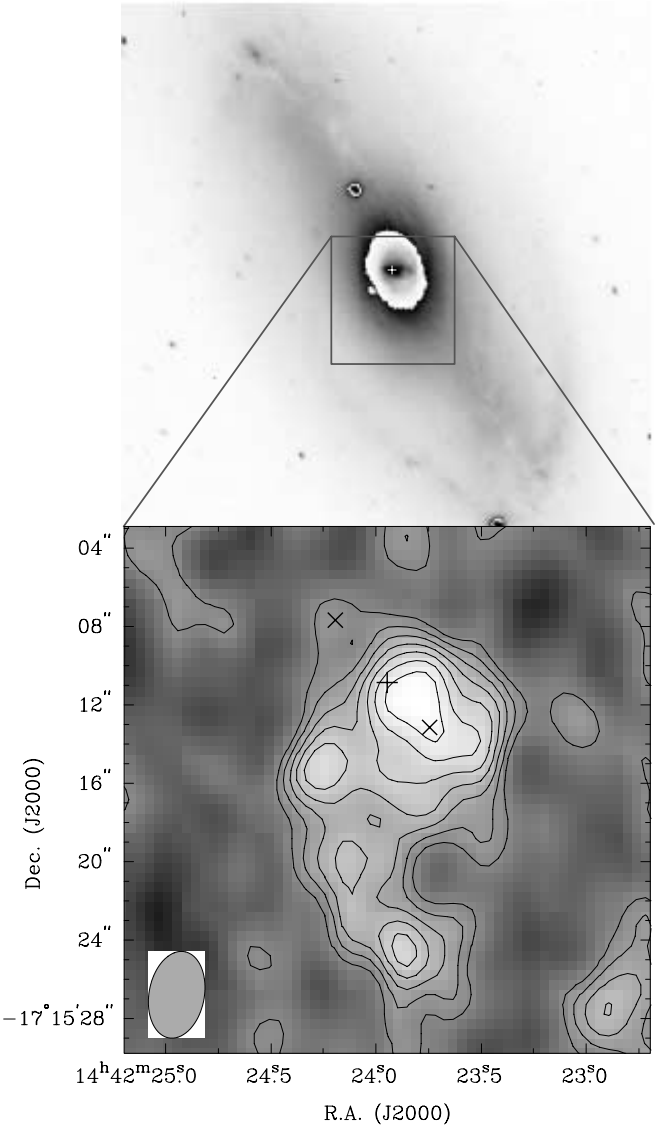

FIG. 5.—^{12}CO $J = 1$–0 integrated intensity map for the nucleus of NGC 5728 (*bottom panel*). Note that we do *not* see a secondary gas bar as we do for NGC 2273. The top panel shows the composite *I*-band image from Prada & Gutiérrez (1999) indicating the location of the nuclear stellar bar. The CO emission appears be asymmetric with respect to the dynamical center of the galaxy (marked by the plus sign) determined by Schommer et al. (1988). The rms noise in the map is 2.65 Jy beam^{-1} km s^{-1}, and the contours start at 0.5 σ and increase in steps of 0.5 σ. The beam size is $4\farcs5 \times 3''$, with a P.A. $= -12°$, and is shown in the lower left corner. The crosses indicate the clumps used to determine the dynamical mass in § 3.2.

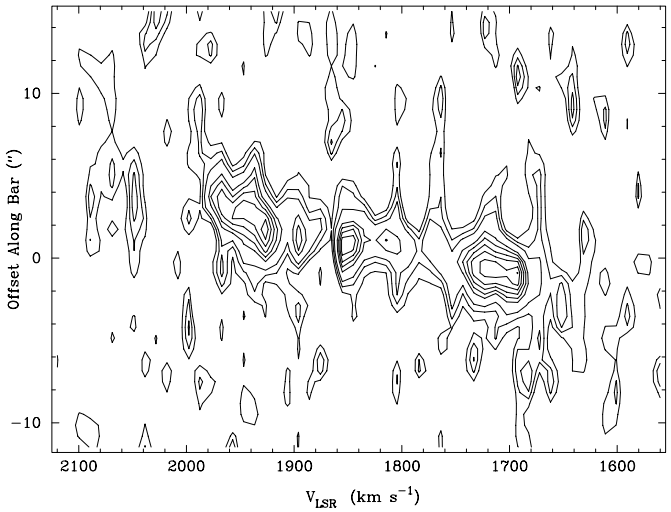

FIG. 6.—Position-velocity diagram for a slice along the major axis of the CO bar in NGC 2273 shown in Fig. 2. It rotates as a solid body with a projected velocity gradient of 570 km s^{-1} kpc^{-1}. Contours indicate 10%, 20%, 30%,. . . of the peak. Positive offsets are toward the northeast end of the bar.

galaxy's inclination, and G is the gravitational constant. Contributions from noncircular velocities can only cause deviations of approximately 30% in the calculated mass (e.g., Sakamoto et al. 1999). Using Figure 4 to obtain velocities at the bar ends and assuming the inclination to be 41°, we find the dynamical mass of the nuclear molecular bar to be $1.6 \times 10^9\ M_\odot$.

The channel maps of NGC 5728 (Fig. 7) show a much less ordered appearance than in NGC 2273. Careful examination of the velocity of the clumps suggests that the southernmost clump has the highest recession velocity, and the velocities of the clumps decrease as you move clockwise around the arc (ignoring the CO emission associated with the dust lane to the far south). This is consistent with the velocity field determined by the Hα maps of Schommer et al. (1988). The CO emission is very clumpy, with some of the features seen in the integrated intensity map of Figure 5 being made up of numerous CO features that are separated in velocity space. The brightest peak is actually a superposition of many fainter peaks at different velocities. There is no evidence in our CO maps of NGC 5728 for a bar interior to the ring, as reported by Prada & Gutiérrez (1999), so naturally we cannot confirm the reports that this secondary bar may be counter-rotating.

Our CO data for NGC 5728 are not sufficient to create a high-quality position-velocity map as we did for NGC 2273, but we can use the channel maps to determine the position and velocity for the two bright clumps that lie nearly along the kinematic major axis of NGC 5728 and straddle the dynamical center.[2] Using the same equations as for NGC 2273, we calculate a dynamical mass of $6.3 \times 10^9\ M_\odot$ for the inner 8″ of NGC 5728. We note that since there is no strong evidence for circular motion in the CO maps, there is extremely high uncertainty associated with this value. An alternative value for the dynamical mass of the inner kiloparsec of NGC 5728 is given in the next section.

4. MOLECULAR GAS MASS AND GAS MASS FRACTION

We use the CO flux over the entire nuclear bar of NGC 2273 to estimate the molecular gas mass in the nuclear region. We adopt

$$M_{\rm gas} = 1.6 \times 10^4 \left(\frac{D}{\rm Mpc}\right)^2 \left[\frac{S_{\rm CO(1-0)}}{\rm Jy\ km\ s^{-1}}\right] \left(\frac{X}{X_{\rm Gal}}\right)$$

(Wilson 1995), where D is the distance to the galaxy, $S_{\rm CO(1–0)}$ is the ^{12}CO $J = 1$–0 flux, and X is the CO-to-H$_2$

[2] The northeast peak is at R.A. $= 14^{\rm h}42^{\rm m}24\fs2$, $\delta = -17°15'07\farcs6$ and has a central velocity of 2660 km s^{-1}. The southwest peak is at R.A. $= 14^{\rm h}42^{\rm m}23\fs75$, $\delta = -17°15'13\farcs0$ and has a central velocity of 2960 km s^{-1}. These points are indicated in Fig. 5 by crosses.

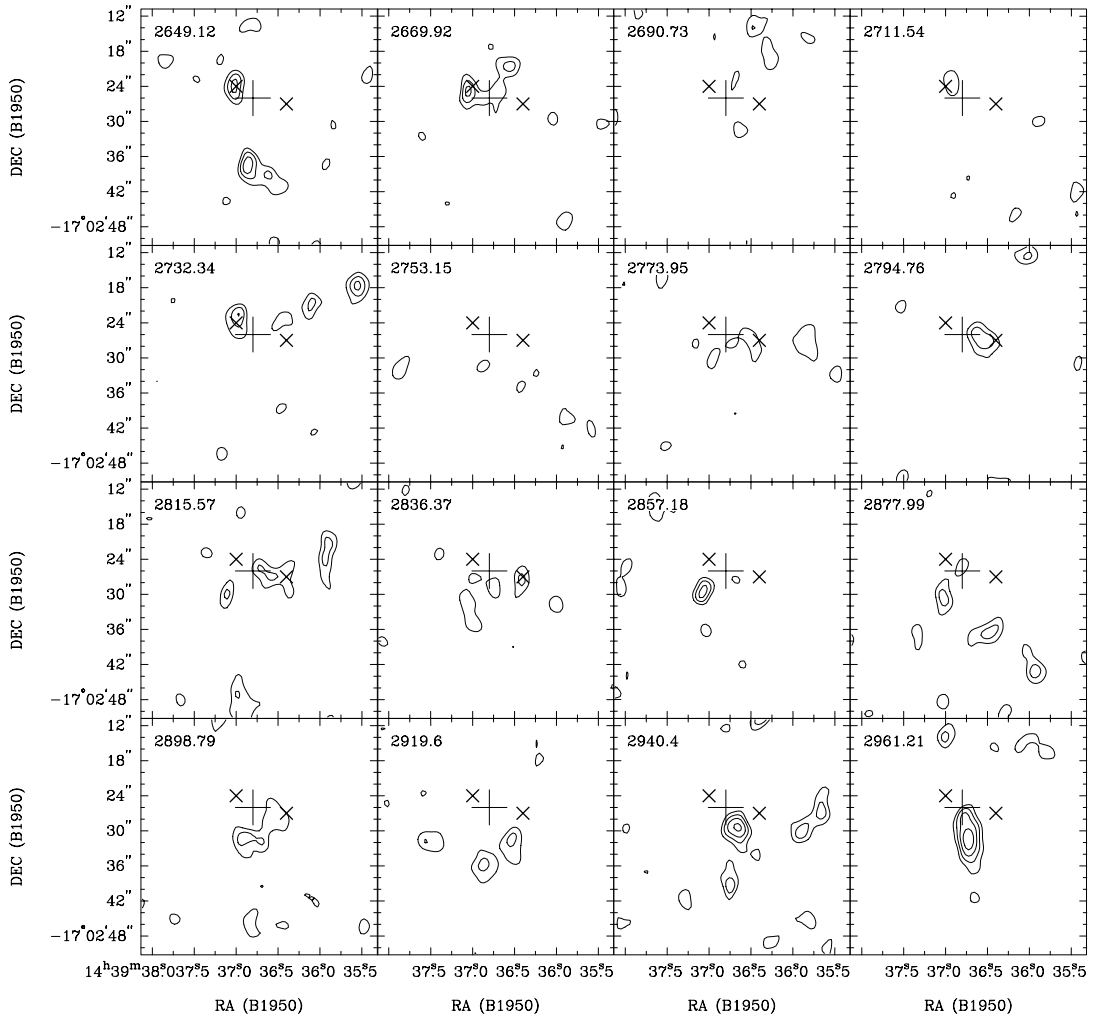

FIG. 7.—Channel maps of NGC 5728. Note how there is not strong evidence for large-scale ordered motion. The large plus sign indicates the galaxy center determined by Schommer et al. (1988). The smaller crosses mark the locations of the peaks used to calculate the dynamical mass. Contour levels are 0.04, 0.06, 0.08,... Jy beam^{-1} (1.5, 2.3, 3,... σ). The panels are shown at 20.8 km s^{-1} intervals and are binned to 20.8 km s^{-1} wide bins.

conversion factor compared to the Galactic value ($X_{\rm Gal}$). The constant at the start of the equation contains a factor of 1.36 to account for other elements besides hydrogen. For lack of evidence to the contrary, we adopt the Galactic value of the CO-to-H_2 conversion factor of 3×10^{20} cm^{-2} (K km s^{-1})$^{-1}$ (Scoville & Sanders 1987) for the galaxies studied in this paper. The total CO flux for the nuclear CO bar of NGC 2273 is 48.6 Jy km s^{-1}, which corresponds to a molecular mass of 4.7×10^8 $M_\odot$. If we repeat this calculation using only the region interior to the locations used in the dynamical mass calculation ($\sim$1 kpc along the length of the CO bar), we measure a flux of 38.0 Jy km s^{-1} (uncorrected for primary beam falloff), which corresponds to a molecular mass of 3.6×10^8 $M_\odot$. This mass constitutes approximately 20% of the galaxy's dynamical mass within this radius (§ 3.2).

Of course, the estimate for the molecular gas mass is only a lower limit, since the interferometer is insensitive to the large-scale structure that may be present in the nuclear regions of this barred galaxy. Single-dish ^{12}CO $J = 1$–0 spectra of the inner 55″ of NGC 2273 taken by Young et al. (1995) show a flux of 137 ± 24 Jy km s^{-1}, suggesting that our interferometry maps may be missing up to 65% of the CO emission. Also important is the effect of the uncertainties in the individual measurements used to calculate this ratio. For example, in § 3.2, if we assume that $V_{\rm circ}$, i, and R each have a conservative $\sim$10% uncertainty, this results in a $\sim$25% uncertainty in $M_{\rm dyn}$. Similarly, for the molecular gas mass, if we assume a $\sim$10% uncertainty for each measured value, we obtain an uncertainty in $M_{\rm gas}$ of $\sim$20%. The final value for the ratio $M_{\rm gas}/M_{\rm dyn}$ is (20 ± 6)%.

Yankulova (1999) finds that the nuclear ring of NGC 2273 is very dusty and calculates the mass of this dust to be $\sim 10^5$ $M_\odot$. Comparing this to our molecular gas mass, we find that the gas-to-dust ratio is approximately 3600 in the center of this Seyfert 2 galaxy. This ratio is higher than found for nearby spiral galaxies ($M_{\rm gas}/M_{\rm dust} \sim 1000$; Devereux & Young 1990). It may not be surprising that the ratio of gas to dust is higher in the center of this barred galaxy, where we might expect an increase of nuclear molecular gas (caused by inflow along the bar) as well as a decrease in dust due to the strong ionizing nuclear source (Yankulova 1999).

The CO flux for the inner 8″ × 8″ of NGC 5728 is 25.6 Jy km s^{-1} (uncorrected for primary beam falloff), which indi-

cates a molecular mass of $5.7 \times 10^8\ M_\odot$. Using our dynamical mass data, we find that the molecular gas in the nucleus of NGC 5728 constitutes 9% of the total mass. We believe that our determination of the dynamical mass in such a complicated environment is likely to be unreliable. Our dynamical mass determined in § 3.2 is lower than the value determined by Rubin (1980) through model fits of the velocity data over the entire galaxy. Because of the complexity of our data and the simplicity of the models assumed in § 3.2, we adopt the value determined by Rubin (1980). She finds that the total dynamical mass of the galaxy in the inner 10″ diameter (1.8 kpc) is $\sim 1 \times 10^{10}\ M_\odot$. This estimate lowers the mass fraction of molecular gas to (6 ± 2)%. Again, this result is a lower limit, because the interferometer will miss large-scale structure. There are no single-dish ^{12}CO $J = 1$–0 spectra for NGC 5728 published, so we cannot directly estimate the flux missed by our interferometric maps. Single-dish ^{12}CO $J = 2$–1 spectra of the inner 22″ of NGC 5728 (G. R. Petitpas & C. D. Wilson 2002, in preparation) show fluxes of 62 Jy km s^{-1}. Assuming a ^{12}CO $J = 2$–1/$J = 1$–0 flux ratio of 2.8 (Sakamoto et al. 1995), we obtain a ^{12}CO $J = 1$–0 flux of 22 Jy km s^{-1}. Comparing this to the CO flux in the interferometric map of 30 Jy km s^{-1} for this region, we find that the interferometric maps are detecting all of the flux detected by a single dish.

The models of both Shaw et al. (1993) and Friedli & Martinet (1993) must contain molecular gas in order to create and sustain nuclear bars and twists. Friedli & Martinet (1993) found that they could create nuclear bars if the *total* (atomic+molecular) gas to total mass ratio is 10%, or if 2% of the total mass interior to 1 kpc (diameter) is molecular. Shaw et al. (1993) were less specific and only stated that 4%–6% of the entire galaxy mass needs to be gaseous; a large portion of this gas is presumably transferred inward at later stages, but specific values are not quoted. The high gas contents in these two models are required to provide enough dissipation so that the nuclear ring can become phase shifted out of its stable orbit and collapse into a nuclear bar or twist out of alignment. Both galaxies meet the initial nuclear molecular gas mass requirements of Friedli et al. (1996), yet only NGC 2273 shows evidence for a nuclear molecular bar. It is interesting that we find ~20% gas (by mass) in the nucleus of NGC 2273, where we see a nuclear bar, yet we only see ~6% (by mass) in the nucleus of NGC 5728, where we see no evidence in our CO maps for a nuclear bar. We defer discussion on potential reasons for the differences to §§ 6 and 7.

A recent interferometric ^{12}CO $J = 1$–0 survey by Sakamoto et al. (1999) suggests that typical gas mass fractions range from 0.9% to 31.5% in the inner 500 pc radius of a sample of 17 galaxies, with no apparent correlation with galaxy type. Since we have used the same techniques to determine the gas mass fraction, it is worthwhile to compare our results with those of a larger sample. For NGC 2273, we calculate the molecular gas mass fraction over the entire length of the bar for which we see emission in the position-velocity plot (Fig. 6), which corresponds to the inner 720×720 pc. For NGC 5728, we measured the molecular gas mass fraction over an area of $8'' \times 8''$, which corresponds to the inner 1.4×1.4 kpc. NGC 2273 has a nuclear gas mass fraction of 20%, and NGC 5728 has 6% molecular gas. Sakamoto et al. (1999) find evidence that H II nuclei have higher ratios of gas to dynamical masses (~18% average) compared to Seyfert and LINER galaxies (~6% average). NGC 5728 is in agreement with the previously observed range for its type of nuclear activity, while NGC 2273 seems to have a higher molecular gas fraction than the other Seyfert 2 galaxies in the sample obtained by Sakamoto et al. (1999). A distinct classification of NGC 2273 into one particular category is difficult in light of observations that suggest that in addition to its Seyfert 2 activity, NGC 2273 is undergoing nuclear star formation (Mulchaey et al. 1996). These observations suggest that NGC 2273 may be an intermediate object that should fall somewhere between the H II and the Seyfert 2 classifications of Sakamoto et al. (1999), in which case it is in the expected intermediate range of gas mass fraction for such an object. In any case, our observed gas mass fraction for NGC 2273 does not compromise the results of Sakamoto et al. (1999).

Thus far, we have concentrated our comparisons predominantly on the models of double-barred galaxies that are composed of both stars and gas. There is another class of models that attempt to explain nuclear NIR isophote twists using purely stellar orbits (Maciejewski & Sparke 2000). It is known that there are different classes of orbits in a barred potential. The two important ones are the x_1 family that runs parallel to the bar major axis and the x_2 family, which runs perpendicular to it (e.g., Athanassoula 1992). It was thought that the x_2 orbits of the large-scale bar near the nucleus could form the x_1 orbits of the smaller nuclear bar, and the corotation radius of the nuclear bar could correspond to the ILR of the large-scale bar. In this picture, the nuclear bar must *always* be aligned perpendicular to the primary bar. Friedli & Martinet (1993) rule out this model by studying a large sample of double-barred galaxies, since they found that not all the observed offset angles between the nuclear bar and the primary bar can be explained by inclination effects. Recently, Maciejewski & Sparke (2000) found that there exist orbits in which particles in a double-barred potential remain on closed orbits and may form the building blocks of long-lived double-barred galaxies without the need for a gaseous component. The particle nature of this model renders it untestable with our molecular gas observations, since molecular gas will not orbit in a particle-like manner. We mention it here solely as a possible explanation of why NGC 5728 shows a nuclear stellar bar in the NIR images but no nuclear bar in the CO maps.

5. INFLOW AND GAS CONSUMPTION IN NGC 2273

Since nuclear bars are believed to be responsible for the inflow of molecular gas, we may expect to see signs of inflow in the CO observations of NGC 2273. In Figure 8, we show the velocity field (moment 1 map) for NGC 2273 superimposed on the integrated intensity CO map. The lines of constant velocity start at 1700 km s^{-1} (the broken contour in the southeast) and continue up to 1980 km s^{-1} (the very short, westernmost contour) in increments of 20 km s^{-1}. The white line is the 1 σ integrated intensity contour from Figure 2.

The velocity field does not show evidence of the characteristic S-shaped contours indicative of inflowing molecular gas. One possible explanation for this is that we are probably not resolving the bar across the minor axis. The contours are nearly parallel across the major axis and are evenly spaced, which is consistent with solid-body rotation. The kinematic major axis of the nuclear bar aligns with the kinematic major axis of the rest of the galaxy, as seen in the H I

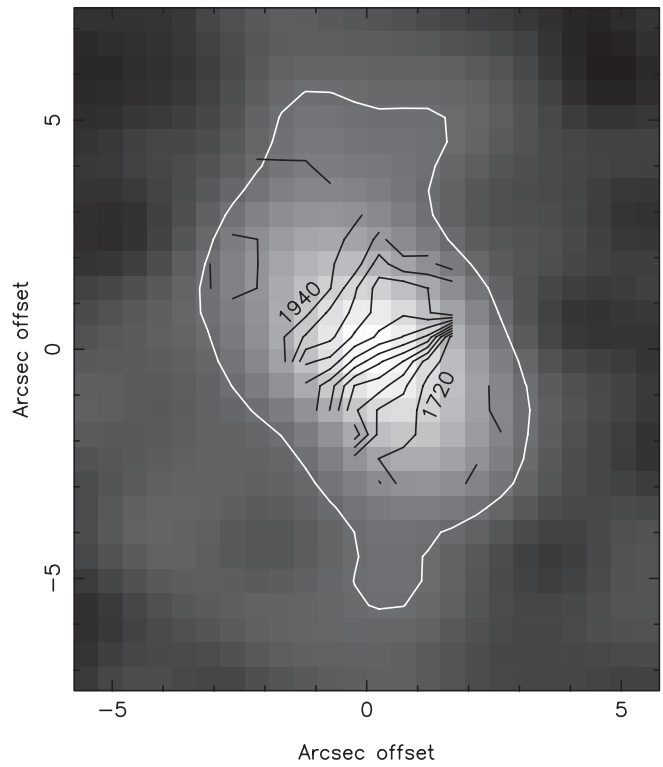

FIG. 8.—Moment 1 map for the CO bar of NGC 2273. The black lines are lines of constant velocity, ranging from 1700 to 1960 km s^{-1} in increments of 20 km s^{-1}. The underlying gray scale is the CO integrated intensity map, and the white contour is the 1 σ contour from Fig. 2.

maps of van Driel & Buta (1991). A signature similar to this is seen in the unresolved nuclear gas bar of NGC 3351 (Devereux et al. 1992). Another explanation for the lack of kinematic signs of inflow is that the molecular gas may be contained solely within the three independent gravitationally bound clumps seen in Figure 4. If this is the case, then there would not be sufficient inflowing material to be detected by our interferometric observations.

If the molecular material is confined to individual clumps surrounding the nucleus, we might ask if the dynamical drag on these clumps may be an effective means of transporting molecular material deep into the nucleus. The masses of the individual clumps are on the order of $6 \times 10^7\ M_\odot$, much smaller than the dynamical mass of the galaxy interior to these clumps ($\sim 1.5 \times 10^9\ M_\odot$; from Fig. 4), which suggests that dynamical friction resulting from the background stellar population may be an effective means of transporting material into the nuclear regions. The dynamical friction timescale can be written

$$f_{\rm fric} = \frac{2.64 \times 10^8}{\ln \Lambda} \left(\frac{r}{\rm pc}\right)^2 \left(\frac{v}{\rm km\ s^{-1}}\right) \left(\frac{M_\odot}{M}\right) ,$$

where we have assumed an isothermal sphere density distribution, and r and v are the orbital properties of a cloud with mass M. Here Λ is the Coulomb logarithm and can be expressed

$$\Lambda = 230 \left(\frac{b}{\rm pc}\right) \left(\frac{v}{\rm km\ s^{-1}}\right)^2 \left(\frac{M_\odot}{M}\right)$$

(Binney & Tremaine 1987; Jogee et al. 1999), where b is the effective radius of the cloud from the galaxy center.

For the two outer clumps in the nuclear gaseous bar of NGC 2273 (masses $\sim 6 \times 10^7\ M_\odot$) moving with an average velocity of 180 km s^{-1} (deprojected) at a radius of 200 pc (the average of the outermost clumps in Fig. 4), we estimate the timescale for dynamical friction to be 10^7 yr. This timescale is shorter than the predicted lifetimes of nuclear bars ($\sim$few $\times 10^8$ yr; Friedli & Martinet 1993), which suggests that dynamical friction may be an effective means of transporting molecular gas into the nucleus of NGC 2273 and in turn will likely affect the evolution of the nuclear bar in this galaxy. The combined mass of the two outer CO clumps is approximately $1 \times 10^8\ M_\odot$. Assuming that all of this gas is transported inward through dynamical friction, we estimate the inflow rate to be on the order of 10 $M_\odot$ yr^{-1}. We note that this value will be modified if in fact we are not resolving the CO emission. Smaller clumps will have smaller masses and thus longer timescales. Conversely, clumps at smaller radii will have much shorter timescales, so if in fact the individual clumps used in this analysis are actually comprised of smaller clumps at a range of radii, our estimate of the dynamical timescale will have to be altered accordingly.

It is interesting to compare the above inflow estimate with the star formation rates predicted from the infrared luminosity of the nuclear starburst in NGC 2273. Following Hunter et al. (1986) and assuming the infrared luminosity ($\log L_{\rm FIR}/L_\odot = 10.11$; Bonatto & Pastoriza 1997) comes from dust heated by the nuclear star formation seen in the Hα maps of Sánchez-Portal et al. (2000), we estimate star formation rates in the nuclear bar of NGC 2273 to be $\sim$3–6 $M_\odot$ yr^{-1}. This value is in good agreement with the inflow rates derived from dynamical friction arguments. Assuming that all the molecular gas detected with the interferometer (namely, the gas in the dense clumps) is used, there is enough material to feed these star formation rates for 10^8 yr. This lifetime is approximately the same or shorter than the predicted lifetime of the nuclear bars in the simulations of Friedli & Martinet (1993), indicating that star formation will play an important role in the evolution of double-barred galaxies.

The star formation and gas inflow rates in NGC 2273 are very similar to the values obtained for NGC 2782 using similar techniques (Jogee et al. 1999). Both the high star formation rates and the high inflow rates in these two galaxies, which contain both nuclear gaseous and nuclear stellar bars, suggest that gas-rich nuclear bars are a very effective means of transporting gas into the nuclear regions, where it may fuel star formation and perhaps other forms of nuclear activity. We note as a counterexample the double-barred galaxy NGC 4736 (Wong & Blitz 2000). It contains both a nuclear stellar and a gaseous bar (although somewhat weaker than NGC 2273), yet it has a nuclear star formation rate of only 0.2 $M_\odot$ yr^{-1}. We will need more observations of similar galaxies to build up a large enough sample to draw any strong general conclusions.

6. COMPARISON TO OBSERVATIONS AT OTHER WAVELENGTHS

6.1. *NGC 2273*

It has long been known that large-scale bars are a good way to transport material into the nuclear region of a galaxy

(e.g., Combes 1994) by allowing material to flow inward along the leading edge of the bar. Indications of such an inflow along the large-scale bar are visible in the CO map of NGC 2273, seen as fingers extending northwest and southeast from the top and bottom, respectively, of the CO bar. This observation suggests that inflow along the primary bar of NGC 2273 is depositing material onto the ends of the nuclear bar seen in the CO maps. This material would then be free to flow along the nuclear bar into the central regions and could possibly supply the nucleus with enough material to sustain the observed Seyfert and starburst activity. It is possible that the large-scale bar will resupply the nuclear bar with molecular material, allowing it to live longer than predicted in § 5, when we assumed that the material in the bar was all that was available to the nuclear starburst.

The channel maps of NGC 2273 show that the bar seen in the integrated intensity maps is actually composed of three separate structures. These structures are barely spatially resolved in our maps (if at all), but they are clearly resolved in velocity (as seen in Fig. 3). Similar nuclear CO distributions have been seen previously in single-barred galaxies such as NGC 5383 and M82 (Sheth et al. 2000; Neininger et al. 1998). In NGC 5383, Sheth et al. (2000) see bright CO emission from "twin peaks" that coincide with the ILR radius, as well as a central concentration near the nucleus. High-resolution observations suggest that the nuclear structure of NGC 5383 is actually a nuclear spiral when viewed with the *HST* (Sheth et al. 2000), which casts some doubt on the identification of nuclear bars with lower resolution ground-based images.

HST images (Malkan, Gorjian, & Tam 1998) and narrowband color maps (Yankulova 1999) of NGC 2273 show that the nucleus contains a ring elongated in the same direction as our nuclear CO bar. The *HST* (WFPC2, F606W) images show a central bright spot and indications of what may be flocculent spiral arms interior to the ring. The bright blobs at the ends of the nuclear CO bar correspond with the edges of the ring seen by Malkan et al. (1998) and Yankulova (1999). It is likely that this ring indicates the location of the ILR of the primary bar, and thus, our nuclear bar ends occur at the ILR radius, as predicted by the models of Friedli & Martinet (1993) and Shaw et al. (1993).

6.2. *NGC 5728*

HST images of the nucleus of NGC 5728 show what appears to be an off-center ring of young stars circling two ionization cones that seem to originate from a point $\sim 3''$ west-northwest (-60°) from the center of our maps (Wilson et al. 1993). These images also show a barlike structure that is oriented at a position angle of $\sim 90^\circ$, which Wilson et al. (1993) suggest may be composed of older stars. Our CO map shows no bright emission peak at the vertex of the ionization cones of the *HST* maps. The bright and faint CO peaks (used in § 3.2 to determine the dynamical mass) that straddle the map center are roughly perpendicular to the ionization cones. The other peaks in the maps (curving to the south) are associated with the dust lanes that run along the leading edge of the primary bar (Schommer et al. 1988). Our CO maps also do not show any strong evidence of a bar structure oriented at P.A. $=\sim 90^\circ$, which might correspond to the bar suggested by the NIR images of Shaw et al. (1993). If we assume that the clumps (Fig. 5, *crosses*) that straddle the dynamical center (*plus sign*) correspond to similar nuclear bar end enhancements as seen in NGC 2273 (Fig. 2), then the nuclear CO bar in NGC 5728 would be leading the stellar nuclear bar seen in the NIR images by $\sim 45^\circ$. This angle is greater than the offsets predicted by Shaw et al. (1993) and Friedli & Martinet (1993) for which a 20° maximum offset is predicted. If the nuclear stellar bar is counter-rotating as reported by Prada & Gutiérrez (1999), then the nuclear CO bar is trailing the primary bar, which is only predicted in kinematically distinct nuclear bar models of Friedli & Martinet (1993).

Unfortunately, the integrated intensity maps and the channel maps of the nucleus of NGC 5728 show no *conclusive* evidence for a nuclear bar in our data either aligned or misaligned with the NIR isophote twists. This result suggests that if the NIR isophote twists of Shaw et al. (1993) are the result of a nuclear bar, it is mostly stellar and contains little molecular gas. This suggests that there is a possibility that the molecular gas distribution has been modified by star formation activity, and future models of double-barred galaxies may need to include the effects of star formation. This scenario is elaborated on in the following section.

Another (more likely) possibility is that the off-center CO emission seen in NGC 5728 may be evidence of a recent merger event. The lack of tidal tails suggests that any merger experienced by NGC 5728 would have been a minor merger. Simulations of minor mergers by Hernquist & Mihos (1995) show evidence for molecular gas offset from the primary galaxy center. If the asymmetric CO map is the result of a minor merger, it may be responsible for triggering the large-scale bar perturbation and could account for the counter-rotating core reported by Prada & Gutiérrez (1999). Minor mergers have been attributed as the possible cause of the X-shaped S0 galaxies (Mihos et al. 1995), and the similarities between these X-structures and the NIR isophote twists seen in NGC 5728 are noteworthy.

7. COMPARISONS WITH OTHER CANDIDATE DOUBLE-BARRED GALAXIES

From the NIR surveys that have detected the isophote twists originally thought to be the signature of a nuclear bar (e.g., Mulchaey et al. 1997; Shaw et al. 1993; Wozniak et al. 1995; Jarvis et al. 1988; Elmegreen et al. 1996; Friedli & Martinet 1993; Jogee et al. 1999), only a handful of galaxies have high-resolution CO maps published: NGC 2273, NGC 5728, NGC 2782, NGC 4736, and NGC 6951 (this work; Jogee et al. 1999; Sakamoto et al. 1999; Kenney et al. 1992). NGC 2273, NGC 2782, and NGC 6951 contain two peaks at the ILR radius with more CO emission interior to these peaks. CO maps of NGC 4736 show what may be a weak twin peak structure, with a bright central concentration (Sakamoto et al. 1999). NGC 5728 has a bright, off-center peak of emission, with other emitting regions that do not seem to line up with other features or the ILR radius. Only NGC 5728 does not show evidence for a twin peaked or bar structure elongated in the same direction as the nuclear NIR isophote twists (possibly as a result of the merger scenario discussed above).

To explain the variety of CO distributions seen in these galaxies, we must first consider the time evolution of the models. The models of Shaw et al. (1993) were only run until they reached a steady state, so comparisons of our CO maps with the predictions for the lifetimes of nuclear bars is not possible. Friedli & Martinet (1993) show that after the

TABLE 2
PROPERTIES NIR ISOPHOTE TWIST GALAXIES

Galaxy	M_{gas}/M_{dyn} (nuclear) (%)	Nuclear Activity	Nuclear CO Morphology	References
NGC 2273.....	20	Star formation, Seyfert 2 activity	Bar/triple peaks	1, 2
NGC 2782.....	8	Star formation, Seyfert 1 activity	Bar/twin peaks	3
NGC 4736.....	2	Star formation in ring outside nucleus, LINER	Central peak, weak signs of twin peaks?	4, 5
NGC 5728.....	6	Evidence of past star formation, Seyfert 2	Noncentralized peaks, no bar	1, 6
NGC 6951.....	29	Star formation	Twin (triple?) peak/ elongated ring?	7

REFERENCES—(1) This paper; (2) Mulchaey et al. 1996; (3) Jogee et al. 1999; (4) Sakamoto et al. 1999; (5) Kinney et al. 1993; (6) Wilson et al. 1993; (7) Kohno et al. 1999.

nuclear bar forms, it usually remains present for over 5 turns of the nuclear bar (approximately 2 turns of the primary bar; ~500 Myr). The double-bar phase can transport the molecular gas inward, which eventually results in the disruption of the nuclear bar; often even the large-scale bar is disrupted by bulge growth (Pfenniger & Norman 1990) or central mass concentration (Hasan & Norman 1990). At all times in these simulations, the gas distribution resembles the stellar distribution, even if they are somewhat out of phase, so the models are incapable of explaining the observed variety of CO distributions. Neither of the double-barred galaxy models by Shaw et al. (1993) or Friedli & Martinet (1993) include star formation, which is abundant in this sample of galaxies and will likely have a strong effect on the molecular gas properties within their nuclear regions.

If we consider the star formation activity of each of these galaxies, we see that NGC 2273, NGC 2782, and NGC 6951 have active nuclear star formation, and the CO maps show a lumpy CO bar, an ordered CO bar, and a distorted twin peak structure with faint central concentration, respectively (this paper; Jogee et al. 1999; Kohno, Kawabe, & Vila-Vilaró 1999; Kenney et al. 1992). In NGC 4736, there is no evidence for active star formation in the nucleus, and the CO maps show a bright central concentration (Kinney et al. 1993; Sakamoto et al. 1999). A summary of these observations is given in Table 2. These results suggest that NGC 2273, NGC 2782, and NGC 6951 could perhaps be in later stages of evolution, in which the nuclear molecular gas bar has been less disrupted by star formation. NGC 4736 may not have yet undergone nuclear star formation, so the molecular gas in the nucleus is not yet exhausted or disrupted. In addition, NGC 5728 shows evidence for past star formation, but very little remains ongoing in the nucleus. If the unusual gas distribution is not the result of a merger but past rounds of star formation, then NGC 5728 may have already disrupted or exhausted the nuclear molecular gas, and it has lost its nuclear gas barred appearance, while the nuclear stellar bar remain unaffected. We emphasize that the models of Friedli & Martinet (1993) do not contain star formation and thus show no evidence for such a time-evolutionary sequence proposed here. Paper II will explore the possible influence of star formation on the molecular gas distributions in more detail. The accurate inclusion of star formation in the models will help shed some light on the different CO morphologies observed in the double-barred galaxies.

Another explanation for the variety of CO morphologies may be that there is different physics at work in the molecular gas in each galaxy. It is interesting that the NIR images of all five galaxies look remarkably similar, while the CO maps look remarkably different. The similarity in the NIR images suggests that the stellar distribution in these galaxies is similar. The differences in the CO morphology suggest that there may be something different about the molecular gas in each galaxy, which causes it to respond differently to the galactic stellar potential. We are in the process of analyzing multitransition CO data in order to place constraints on the molecular gas temperatures and densities for the galaxies discussed above. In Paper II of this series, we will present evidence that the gas properties in these galaxies may be responsible for the variety of CO distributions seen.

In closing, we note that the identification of a gaseous nuclear bar may be ambiguous; there may be confusion between what is considered a twin peak galaxy and what is considered a nuclear bar. Galaxies with unresolved twin peaks will appear to have a nuclear CO bar. For example, NGC 3351 is classified as a twin peak galaxy by Kenney et al. (1992) but considered to have a nuclear CO bar by Devereux et al. (1992). Twin peak galaxies are believed to be caused by gas collecting at an ILR as it flows inward along the leading edge of the primary bar of a galaxy (Kenney et al. 1992). These galaxies are thought to be *preventing* molecular gas from reaching all the way into the nucleus, while nuclear bar galaxies are thought to *assist* molecular gas flow into the nucleus by transporting it interior to the ILR (Kenney et al. 1992; Shlosman et al. 1989). We will need a larger sample of galaxies containing unambiguous nuclear bars in order to determine their properties in comparison to twin peak galaxies.

8. SUMMARY

We have mapped the barred galaxies NGC 2273 and NGC 5728 in ^{12}CO $J = 1$–0 with the Owens Valley Radio Observatory Millimeter Array. These galaxies are known to contain NIR nuclear isophote twists, which are thought to be the signature of a nuclear bar. The main results are summarized as follows:

1. In NGC 2273, we see what appears to be a nuclear molecular bar aligned with the nuclear stellar bar, both of which are approximately perpendicular to the large-scale galactic bar. Since they are both perpendicular to the primary bar, we cannot rule out the possibility that we are actually seeing gas and stars populating the x_2-like orbits of the primary bar instead of a nuclear bar. The lack of a detailed rotation curve for the inner regions of NGC 2273 prevents us from determining if this nuclear bar is kinematically separate from the rest of the galaxy.

2. Using dynamical friction arguments, we estimate the inflow rate along the nuclear bar to be 6–10 $M_\odot$ yr^{-1}. This high rate is comparable to the value determined in the double-barred galaxy NGC 2782 (Jogee et al. 1999) and suggests that dynamical friction may be an effective means of transporting molecular gas in the nuclei of galaxies.

3. In the nucleus NGC 5728, we see a series of clumps of emission that do not seem to align with any of the features previously observed at other wavelengths. CO emission is detected coincident with the dust lane to the south of the nucleus. The peak of the CO map is not aligned with the galactic center nor is it located at the center of the offset nuclear ring seen in the *HST* images of Wilson et al. (1993). We do not see evidence for a nuclear bar in the CO maps, which suggests that if there is a real nuclear bar in the NGC 5728, then it must contain little or no molecular gas. It is possible that the NIR isophote twists thought to be the nuclear stellar bar in NGC 5728 are either caused by a triaxial stellar bulge or are scattered light from the jets observed in the *HST* images of Wilson et al. (1993). The asymmetric gas distribution suggests that NGC 5728 may have undergone a minor merger event in its past.

4. We have calculated the molecular gas mass over the entire nuclear bar of NGC 2273 and find that it contains 4.7×10^8 $M_\odot$ of molecular gas. The inner 1.4×1.4 kpc of NGC 5728 contains 5.7×10^8 $M_\odot$ of molecular gas. Assuming Keplerian motion, we find that the dynamical mass of the inner 10″ of NGC 2273 is 1.9×10^9 $M_\odot$, which translates into a molecular gas mass fraction of 20% for the nucleus of NGC 2273. Adopting the dynamical mass value determined by Rubin (1980), we calculate the molecular mass fraction to be 6% in the nucleus of NGC 5728.

5. Both galaxies contain sufficient molecular gas as required by the initial values of the models by Shaw et al. (1993) and Friedli & Martinet (1993; this is presumed to increase with time, but time-dependent values are not quoted). However, we see only a nuclear gas bar in NGC 2273, possibly because of the potential merger history of NGC 5728.

6. The similarity in the NIR images and the differences in the CO maps accumulated for a sample of galaxies with NIR isophote twists suggest that the molecular gas may have different physical properties or is modified by star formation, which allows it to respond differently in similar gravitational potentials. Multiwavelength data have been obtained to test this hypothesis and will be presented in Paper II.

This research has been supported by a research grant to C. D. W. from NSERC (Canada). This research has made use of the NASA/IPAC Extragalactic Database (NED), which is operated by the Jet Propulsion Laboratory, California Institute of Technology, under contract with the National Aeronautics and Space Administration. The Owens Valley Radio Observatory Millimeter Array is operated by the California Institute of Technology and is supported by NSF grant AST 96-13717.

REFERENCES

Athanassoula, E. 1992, MNRAS, 259, 345
Binney, J., & Tremaine, S. 1987, Galactic Dynamics (Princeton: Princeton Univ. Press)
Bonatto, C. J., & Pastoriza, M. G. 1997, ApJ, 486, 132
Combes, F. 1994, in Mass Transfer Induced Activity in Galaxies, ed. I. Shlosman (New York: Cambridge Univ. Press), 170
de Vaucouleurs, G., de Vaucouleurs, A., Corwin, J. R., Buta, R. J., Paturel, G., & Fouque, P. 1991, Third Reference Catalogue of Bright Galaxies (New York: Springer)
Devereux, N. A., Kenney, J. D., & Young, J. S. 1992, AJ, 103, 784
Devereux, N. A., & Young, J. S. 1990, ApJ, 359, 42
Elmegreen, D. M., Elmegreen, B. G., Chromey, F. R., Hasselbacher, D. A., & Bissell, B. A. 1996, AJ, 111, 1880
Friedli, D., & Martinet, L., 1993, A&A, 277, 27
Friedli, D., Wozniak, H., Rieke, M., Martinet, L., & Bratschi, P. 1996, A&AS, 118, 461
Garcia-Burillo, S., Sempere, M. J., Combes, F., & Neri, R. 1998, A&A, 333, 864
Hasan, H., & Norman, C. 1990, ApJ, 361, 69
Hernquist, L., & Mihos, J. C. 1995, ApJ, 448, 41
Hunter, D. A., Gillett, F. C., Gallagher, J. S., Rice, W. L., & Low, F. J. 1986, ApJ, 303, 171
Jarvis, B. J., Dubath, P., Martinet, L., & Bacon, R. 1988, A&AS, 74, 513
Jogee, S., Kenney, J. D. P., & Smith, B. J. 1999, ApJ, 526, 665
Jungwiert, B., Combes, F., & Axon, D. J. 1997, A&AS, 125, 479
Kenney, J. D. P., Wilson, C. D., Scoville, N. Z., Devereux, N. A., & Young, J. S. 1992, ApJ, 395, L79
Kinney, A. L., Bohlin, R. C., Calzetti, D., Panagia, N., & Wyse, R. F. G. 1993, ApJS, 86, 5
Kohno, K., Kawabe, R., & Vila-Vilaró, B. 1999, ApJ, 511, 157
Kormendy, J. 1979, ApJ, 227, 714
Maciejewski, W., & Sparke, L. S. 2000, MNRAS, 313, 745
Malkan, M. A., Gorjian, V., & Tam, R. 1998, ApJS, 117, 25
Mihos, J. C., Walker, I. R., Hernquist, L., Mendes de Oliveira, C., & Bolte, M. 1995, ApJ, 447, L87
Mulchaey, J. S., Regan, M.W., & Kundu, A. 1997, ApJS, 110, 299
Mulchaey, J. S., Wilson, A. S., & Tsvetanov, Z. 1996, ApJ, 467, 197
Neininger, N., Guelin, M., Klein, U., Garcia-Burillo, S., & Wielebinski, R. 1998, A&A, 339, 737
Pfenniger, D., & Norman, C. 1990, ApJ, 363, 391
Prada, F., & Gutiérrez, C. M. 1999, ApJ, 517, 123
Rhoads, J. E. 1998, AJ, 115, 472
Rubin, V. C. 1980, ApJ, 238, 808
Sakamoto, S., Hasegawa, T., Hayashi, M., Handa, T., & Oka, T. 1995, ApJS, 100, 125
Sakamoto, K., Okumura, S. K., Ishizuki, S., & Scoville, N. Z. 1999, ApJ, 525, 691
Sánchez-Portal, M., Díaz, Á. I., Terlevich, R., Terlevich, E., Álvarez Alvarez, M., & Aretxaga, I. 2000, MNRAS, 312, 2
Sault, R. J., Teuben, P. J., & Wright, M. C. H. 1995, in ASP Conf. Ser. 77, Astronomical Data Analysis Software and Systems IV, ed. R. A. Shaw, H. E. Payne, & J. J. E. Hayes (San Francisco: ASP), 433
Schommer, R. A., Caldwell, N., Wilson, A. S., Baldwin, J. A., Phillips, M. M., Williams, T. B., & Turtle, A. J. 1988, ApJ, 324, 154
Scoville, N. Z., Carlstrom, J. E., Chandler, C. J., Phillips, J. A., Scott, S. L., Tilanus, R. P. J., & Wang, Z. 1993, PASP, 105, 1482
Scoville, N. Z., & Sanders, D. B. 1987, Interstellar Processes, ed. D. J. Hollenbach & H. A. Thronson, Jr., ASSL 134 (Dordrecht: Reidel), 21
Shaw, M. A., Combes, F., Axon, D. J., & Wright, G. S. 1993, A&A, 273, 31
Shen, J., & Lo, K. Y. 1995, ApJ, 445, L99
Sheth, K., Regan, M. W., Vogel, S. N., & Teuben, P. J. 2000, ApJ, 532, 221
Shlosman, I., Frank, J., & Begelman, M. C. 1989, Nature, 338, 45
van Driel, W., & Buta, R. J. 1991, A&A, 245, 7
Williams, J. P., de Geus, E. J., & Blitz, L. 1994, ApJ, 428, 693
Wilson, A. S., Braatz, J. A., Heckman, T. M., Krolik, J. H., & Miley, G. K. 1993, ApJ, 419, L61
Wilson, C. D. 1995, ApJ, 448, L97
Wong, T., & Blitz, L. 2000, ApJ, 540, 771
Wozniak, H., Friedli, D., Martinet, L., Martin, P., & Bratschi, P. 1995, A&AS, 111, 115
Yankulova, I. M. 1999, A&A, 344, 36
Young, J. S., & Devereaux, N. A. 1991, ApJ, 373, 414
Young, J. S., et al. 1995, ApJS, 98, 219